Available online at www.sciencedirect.com
SCIENCE DIRECT
Journal of Catalysis 241 (2006) 400–406
JOURNAL OF CATALYSIS
www.elsevier.com/locate/jcat

Promotion of platinum–ruthenium catalyst for electro-oxidation of methanol by ceria

Sheng-Yang Huang, Chia-Ming Chang, Chuin-Tih Yeh *

Department of Chemistry, National Tsing-Hua University, Hsinchu, 30013 Taiwan, ROC

Received 6 January 2006; revised 4 April 2006; accepted 8 April 2006

Available online 19 June 2006

Abstract

In this work, 10 wt% Pt–Ru/C alloy catalysts with and without CeO_2 modification were prepared by wet chemistry and physically characterized by transmission electron microscopy, X-ray diffraction, and inductively coupled plasma–atomic emission spectrometry. The catalytic activity of the prepared catalysts toward anodic oxidation of methanol was examined by cyclic voltammetry (CV). Modification of the Pt–Ru/C catalyst with CeO_2 significantly increased current densities measured by CV. The promotion was attributed to an increased dispersion of alloy particles. However, the extent of promotion depended heavily on the method of catalyst preparation. Evidently, some of the alloy particles did not participate in reaction because they were impregnated into internal pores of carbon support or occluded into the bulk of CeO_2 crystallites codeposited. Accordingly, the anode activity of prepared catalysts should be proportional to the dispersion of alloy particles dispersed and to their accessibility to reactant during reaction. A promoted catalyst with the highest exposure of Pt–Ru nanoalloys exhibited the best electroactivity to methanol oxidation.

Keywords: Methanol decomposition; Cerium oxide; Platinum; Ruthenium; Redox coprecipitation

1. Introduction

The fuel cell is a developing technology that can efficiently convert chemical energy into electrical energy with a negligible emission of pollutants [1]. Among different types of fuel cells under development, the direct methanol fuel cell (DMFC) is distinguished by its low operational temperature and convenient fuel feeding. These features permit a potential application to portable electronics such as cell phones, laptop computers, and video camcorders. In DMFCs, Pt/C-based catalysts are active for the oxidation of methanol at the anode [2–4]. However, the electrochemical activity of platinum crystallites tends to be poisoned by CO intermediates decomposed from methanol. In attempts to reduce the poisoning effect, Pt/C catalysts have been alloyed with other metals, including Ru, Sn, Au, Re, W, Pd, Rh, and Mo [2–6]. Among the different catalysts studied, Pt–Ru/C is considered the best bimetallic catalyst for the anode of DMFCs [7].

A high loading ($\geqslant$30%) of noble metal is generally required by the Pt–Ru/C bimetallic catalysts to attain a decent DMFC power density. The high price of noble metals has been hindering the commercialization of DMFCs. Decreasing the noble metal loading to an economical level for anode catalysts without sacrificing their activity (power density) is therefore a pertinent subject for DMFC development. A conceivable approach to this development is modifying the Pt–Ru/C with appropriate promoters [8].

Ceria has been a widely used promoter for metallic catalysts for catalytic oxidation and electrode reaction. The promoting role of ceria for catalytic oxidation has been attributed to an increased dispersion of supported metal crystallites and stabilization of the support toward thermal sintering [9–11]. In studies of the electrode reaction, incorporation of nanophase ceria into the cathode catalyst of Pt/C has been found to enhance the single-cell performance of direct alcohol fuel cells (DAFCs) [12–14]. In this paper, we report that the activity of the Pt–Ru/C

* Corresponding author. Fax: +886 3 5711082.
E-mail address: ctyeh@mx.nthu.edu.tw (C.-T. Yeh).

0021-9517/$ – see front matter
doi:10.1016/j.jcat.2006.04.020

catalyst toward the anodic decomposition of methanol also was increased by an appropriate promotion with CeO_2.

2. Experimental

2.1. Catalyst preparation

Four monometallic catalysts of Pt_{10}–Ce_x/C with 10 wt% of Pt and varying cerium content (x, in wt% of cerium) were prepared by the coprecipitation method. In the preparation, Pt^{4+} and Ce^{3+} ions in an aqueous solution of $PtCl_4$ (Merck) and $Ce(NO_3)_3{\cdot}6H_2O$ (Fluka) were coprecipitated onto commercial carbon black (Vulcan XC72; SA = 230 $m^2\ g^{-1}$) by 1 M NaOH at pH 8.0. Bimetallic catalysts (intended for 6.7 wt% Pt and 3.3 wt% Ru, with an Pt/Ru atomic ratio of 1.0) of 10 wt% Pt_7Ru_3/C (by coprecipitation) and Pt_7Ru_3–Ce_{20}/C (with 20 wt% of Ce) were also prepared. Three different methods—coprecipitation (CP), sequential precipitation (SP), and impregnation (IM)—were used to prepare the PtRu–Ce/C catalysts. The CP method was similar to the method used to prepare Pt_{10}–Ce_x/C samples using an aqueous solution of three salts [$PtCl_4 + RuCl_3 + Ce(NO_3)_3$]. In the SP method, the carbon black support was first coated by $Ce(OH)_3$ through precipitation of $Ce(NO_3)_3$, then precipitated with Pt and Ru (at pH 8.0). For the IM sample, Pt, Ru, and Ce ions in the three-salt solution was prepared in two steps: an initial impregnation of these ions to carbon black by stirring for 24 h at 340 K, followed by precipitation by 1 M NaOH at pH 8.0. All of the slurries thus obtained were subsequently washed with DI water, dried at 320 K for 24 h, reduced in flowing H_2/N_2 (10/90 vol%) gas at 470 K for 1 h, and then stored as fresh catalysts.

2.2. Catalyst characterization

Physical properties of the freshly prepared catalysts were characterized by inductively coupled plasma–atomic emission spectrometry (ICP-AES), X-ray diffraction (XRD), and analytic transmission electron microscopy (AEM). The XRD analysis was performed on a MAC Science MXP18 X-ray diffractometer over a 2θ range of 20°–80° with Cu-K_α radiation. A tube voltage of 40 kV and a current of 100 mA were used for the scanning. TEM characterization was performed on a JEOL-2010 microscope equipped with a LaB_6 electron gun source operated at 200 kV. Table 1 lists the fresh catalysts prepared for this study, along with their characterization results.

2.3. Cyclic-voltammetric oxidation of methanol

For the cyclic voltammetry (CV) characterization (through a CH Instruments Model 600B device), 20 mg of catalyst powder was added to 200 mg of Nafion (5% in aliphatic alcohols; Du Pont) and then diluted with 2-propanol (Fluka). The resulting slurry was vibrated for 30 min in an ultrasonic bath into ink. A dried ink sample of ∼4 mg was then brushed onto a piece of carbon paper (2 × 2 cm^2; ElectroChem EC-TP1-060) to serve as a catalyst for a working electrode. An electrochemical cell, comprising the working electrode, a platinum counter electrode, an Ag/AgCl reference electrode, and an electrolyte solution of 1.0 M CH_3OH and 0.5 M H_2SO_4 in a 250-mL beaker, was used for all electrochemical measurements. Cyclic potential were swept between 0.0 and 1.2 V (vs. NHE) at a rate of 20 mV s^{-1} at room temperature. The electrolyte was purged with N_2 for 30 min to allow the system to reach a stable state before the current measurement and was protected in N_2 atmosphere at bubbler pressure during the experiments. All of the CV data correspond to 16th cycle (see supporting information).

Table 1
Physical properties characterized for fresh catalysts prepared in this study

Sample name	Metal[a] (wt%)			XRD		TEM	
	Pt	Ru	Ce	d_{CeO_2}	d_M	d_{CeO_2}	d_M
Pt_{10}/C	7.9	–	–	–	3.1	–	2.6
Pt_{10}–Ce_{10}/C	8.7	–	8.5	4.4	[b]	[b]	[b]
Pt_{10}–Ce_{20}/C	7.3	–	15.2	5.4	[b]	[b]	[b]
Pt_{10}–Ce_{30}/C	7.6	–	22.2	7.6	[b]	[b]	[b]
Pt_7Ru_3/C	5.1	2.4	–	–	2.2	–	2.5
Pt_7Ru_3–Ce_{20}/C-CP	5.2	2.4	15.2	5.5	[b]	6.2	[b]
Pt_7Ru_3–Ce_{20}/C-IM	5.3	2.4	16.5	5.8	[b]	6.0	[b]
Pt_7Ru_3–Ce_{20}/C-SP	5.2	2.5	17.7	10.8	[b]	6.5	2.7[c]

[a] Metal composition was determined by ICP-AES.
[b] Size cannot be detected by the detection method.
[c] From crystallite on bare surface of active carbon (without covered by CeO_2).

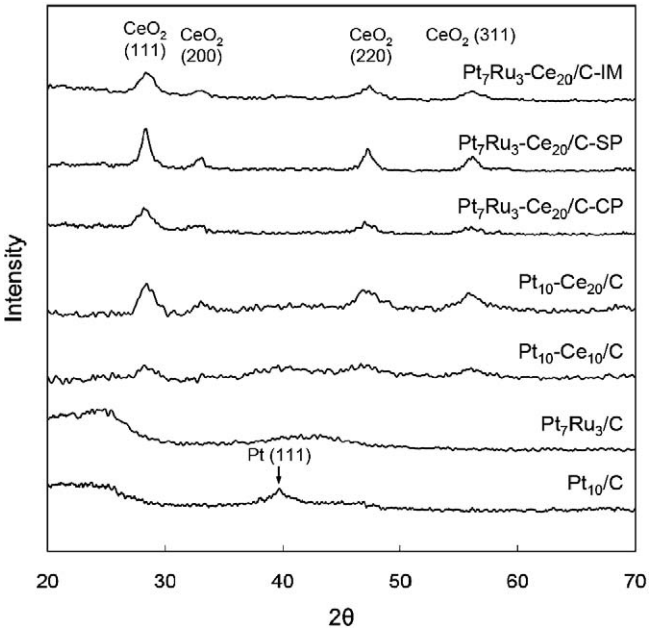

Fig. 1. XRD traces for catalysts freshly prepared and reduced by H_2 at 470 K.

3. Results

Fig. 1 compares XRD traces for the freshly prepared catalysts. Sample Pt_{10}/C shows a peak for Pt (111) at $2\theta = 39.76°$. The width of this peak indicates that the Pt particles in this sample have an average size of $d_{Pt} = 3.1$ nm according to the Debye–Scherrer equation. A broad and weak peak at $2\theta = 42°$ was found in sample Pt_7Ru_3/C. This peak was attributed to dif-

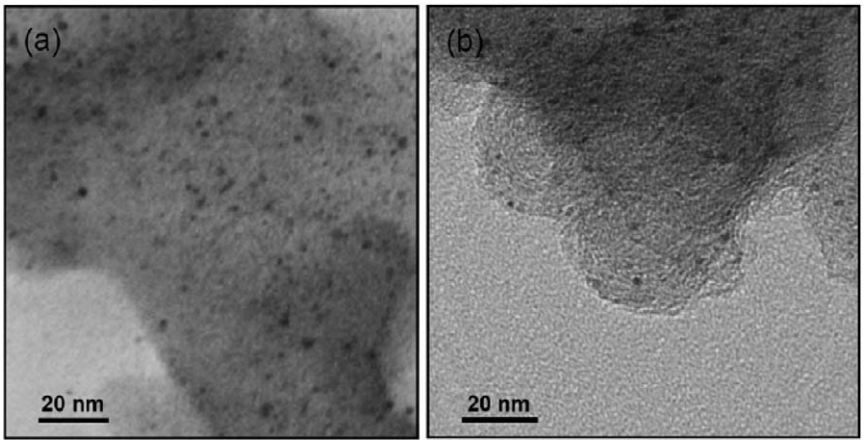

Fig. 2. TEM micrographs of (a) Pt_{10}/C and (b) Pt_7Ru_3/C-CP catalysts. The average particle size of metal was $d_{Pt} = 2.6$ and $d_A = 2.5$ nm.

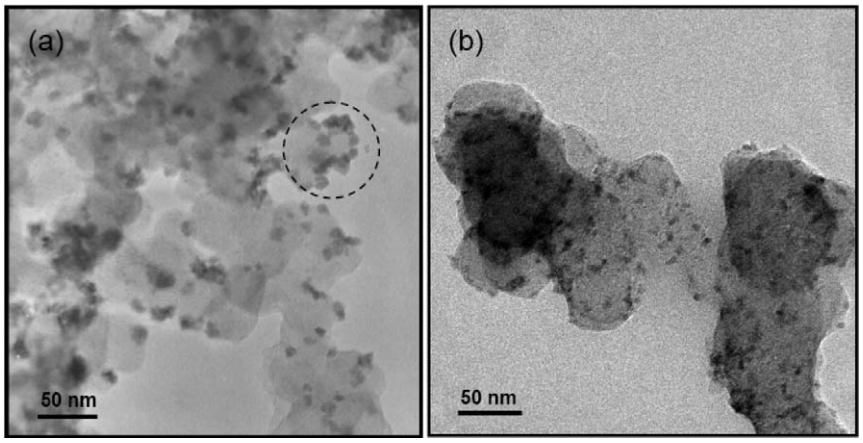

Fig. 3. TEM micrographs of (a) Pt_7Ru_3–Ce_{20}/C-CP and (b) Pt_7Ru_3–Ce_{20}/C-IM. The average particle size of CeO_2 is d_{CeO_2} = (a) 6.2 and (b) 6.0 nm.

fraction of a Pt-rich phase in Pt–Ru alloy (A^{Pt}) [2]. The broad width of the peak suggested an alloy size of $d_A \sim 2.2$ nm. Negligible metal peaks were found in all of the ceria-modified samples of Pt_{10}–Ce_x/C and Pt_7Ru_3–Ce_{20}/C. Conceivably, deposited metals were finely dispersed on these samples and were of size $d_M < 1.5$ nm. In replacement, four diffraction peaks [(111), (200), (220), and (311)] [15] of CeO_2 were observed in ceria-modified samples. The particle size of deposited CeO_2 (d_{CeO_2}) increased from 4 to 8 nm with the loading of ceria:

$$Pt_{10}\text{–}Ce_{10}/C\ (d_{CeO_2} = 4.4\ \text{nm}) < Pt_{10}\text{–}Ce_{20}/C\ (5.4\ \text{nm}) < Pt_{10}\text{–}Ce_{30}/C\ (7.6\ \text{nm}). \quad (1)$$

Columns 5 and 6 of Table 1 summarize the particle sizes of Pt, PtRu, and CeO_2 estimated from XRD findings for the catalysts prepared.

Fig. 2 compares the TEM micrographs for ceria-free catalysts of Pt_{10}/C and Pt_7Ru_3/C-CP. Many fine Pt particles were dispersed on the fresh Pt_{10}/C catalyst (Fig. 2a); the average size of the Pt particles in this sample was $d_{Pt} = 2.6 \pm 1.0$ nm. Pt and Ru were also homogeneously deposited as finely dispersed particles in the Pt_7Ru_3/C-CP sample; the average size of the alloy particles was $d_A = 2.5 \pm 1.0$ nm (Fig. 2b). The d_M observed in these ceria-free samples were in good agreement with those found on XRD (Table 1).

Fig. 3 compares TEM micrographs (with low magnification) for Pt_7Ru_3–Ce_{20}/C-CP and Pt_7Ru_3–Ce_{20}/C-IM. Sphere particles of around $d \sim 6.2$ nm in size were found for the carbon support of Pt_7Ru_3–Ce_{20}/C-CP (Fig. 3a). A comparison with the XRD sizes given in Table 1 indicates that the spheres should be CeO_2 crystallites. Primary CeO_2 particles of the Pt_7Ru_3–Ce_{20}/C-CP tended to be deposited on the surface of the support. The distribution of CeO_2 was quite inhomogeneous; the aggregation is shown in the circled section at the top right of Fig. 3a. The primary particles of CeO_2 in Pt_7Ru_3–Ce_{20}/C-IM were $d_{CeO_2} = 6.0$ nm in size (Fig. 3b). But negligible CeO_2 aggregation was seen in the TEM image of this sample (Fig. 3b). Conceivably, a large fraction of metal and CeO_2 should have been impregnated into the internal pores of active carbon during initial impregnation of the preparation.

Negligible PtRu deposition on the bare surface of active carbon (the light background without CeO_2) can be seen in Fig. 3. In all likelihood, fine alloy particles with $d_M < 1.5$ nm should have been deposited on these samples and incorporated into the lattice CeO_2 structures. This incorporation can be anticipated from the coprecipitation method used, as described in Section 4.

Fig. 4 shows bright-field TEM micrographs for the Pt_7Ru_3–Ce_{20}/C-SP catalyst. Fig. 4a shows an aggregation of CeO_2 particles with $d_{CeO_2} = 6.5$ nm. A high-resolution image of an

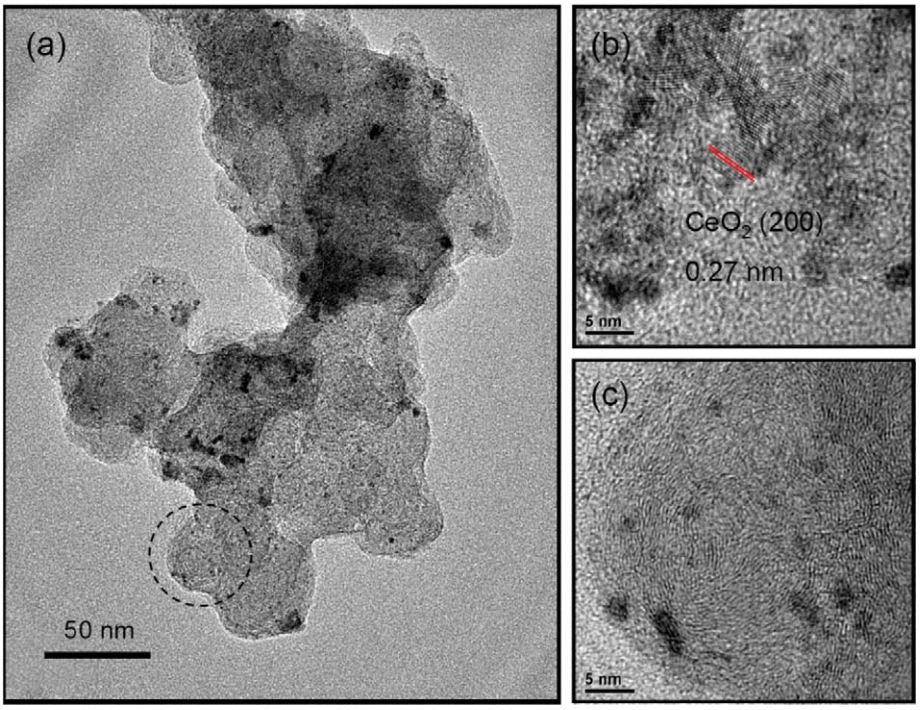

Fig. 4. Bright-field TEM micrographs of Pt_7Ru_3–Ce_{20}/C-SP catalyst. (a) TEM image, (b) high resolution image of CeO_2 deposited surface and (c) high resolution image of PtRu nanoalloys deposited surface. The average particle size of PtRu was $d_A = 2.7$ nm.

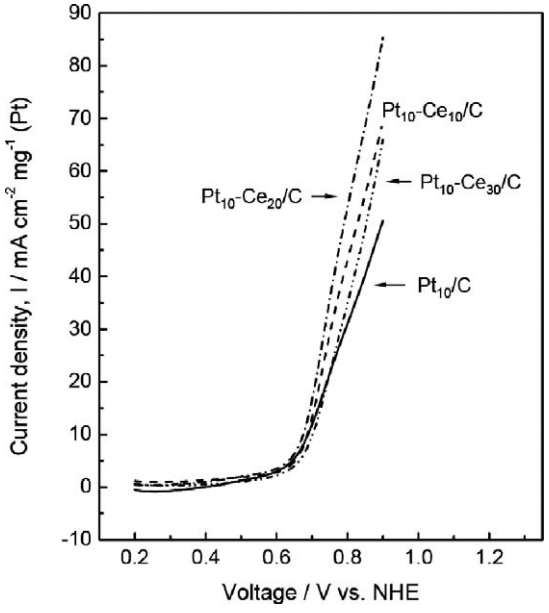

Fig. 5. Cyclic voltammograms of methanol oxidation over Pt_{10}–Ce_x/C catalysts in 1.0 M CH_3OH and 0.5 M H_2SO_4.

aggregation (Fig. 4b) shows lattice fringes of CeO_2(200) with a spacing of 0.271 nm. Fig. 4c (an enlargement of from the circled section in the bottom left of Fig. 4a) displays the image of PtRu nanoalloy particles deposited directly on the bare carbon surface (with no CeO_2 coating). The alloy particles on the bare surface have an average size of $d_M = 2.7 \pm 1.0$ nm. To prepare this SP sample, cerium oxide was precoated on carbon black support before the deposition of metal ions. Accordingly, alloy particles should be deposited on either coated CeO_2 (Fig. 4b) or a bare carbon surface (Fig. 4c). An absent XRD signal (Fig. 1) for alloy particles suggested that the most of the metal components on the Pt_7Ru_3–Ce_{20}/C-SP sample were deposited as fine particles on the coated CeO_2.

Table 2
Catalytic activity of Pt_{10}–Ce_x/C toward methanol oxidation in CV characterization

Sample	E_o[a] (V)	I_{08}[b] (mA cm^{-2} mg$_{Pt}^{-1}$)	E_{max}[c] (V)	I_{max}[d] (mA cm^{-2} mg$_{Pt}^{-1}$)
Pt_{10}/C	0.61	31	0.96	57
Pt_{10}–Ce_{10}/C	0.62	43	1.06	109
Pt_{10}–Ce_{20}/C	0.61	53	1.15	165
Pt_{10}–Ce_{30}/C	0.61	35	1.03	99

[a] E_o: onset potential.
[b] I_{08}: current density at $E = 0.8$ V.
[c] E_{max}: peak potential.
[d] I_{max}: peak current density.

Fig. 5 compares the CVs of methanol oxidation over Pt_{10}–Ce_x/C catalysts in 1.0 M CH_3OH and 0.5 M H_2SO_4. Table 2 summarizes the catalytic performance of these catalysts in the CV characterization. The onset potential of the methanol oxidation is $E_o \sim 0.60$ V (vs. NHE). However, the current density (I) of $Pt_{10}Ce_x$/C was increased on promotion of CeO_2. Fig. 6 summarizes the variation of I_{08} (current density at $E = 0.8$ V) with the stoichiometry, x, of Pt_{10}–Ce_x/C samples. The promotion initially increased with increasing CeO_2 loading; however, an optimized CeO_2 loading of $x \sim 20\%$ was found.

Fig. 7 compares the forward part of CVs on methanol electro-oxidation over the alloy catalyst of Pt_7Ru_3/C-CP with those of CeO_2-promoted Pt_7Ru_3–Ce_{20}/C. Table 3 summarizes the CV characterization from these PtRu alloy catalysts. All of

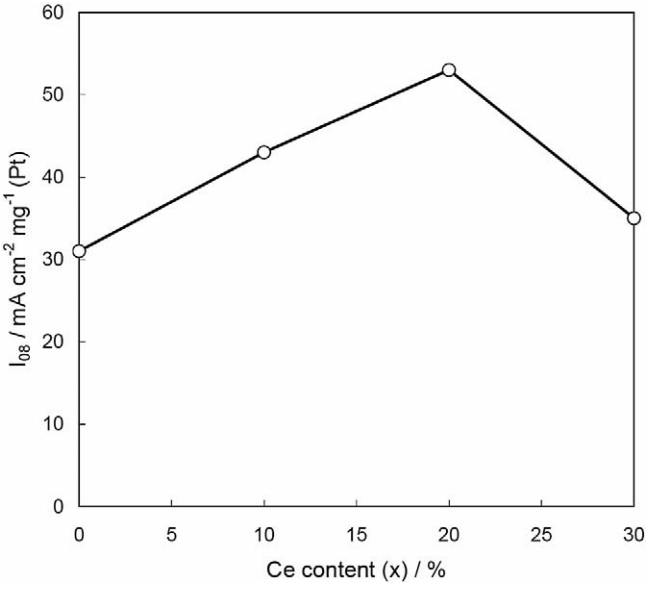

Fig. 6. Variation of I_{08} (current density at $E = 0.8$ V) with the stoichiometry x of Pt_{10}–Ce_x/C samples.

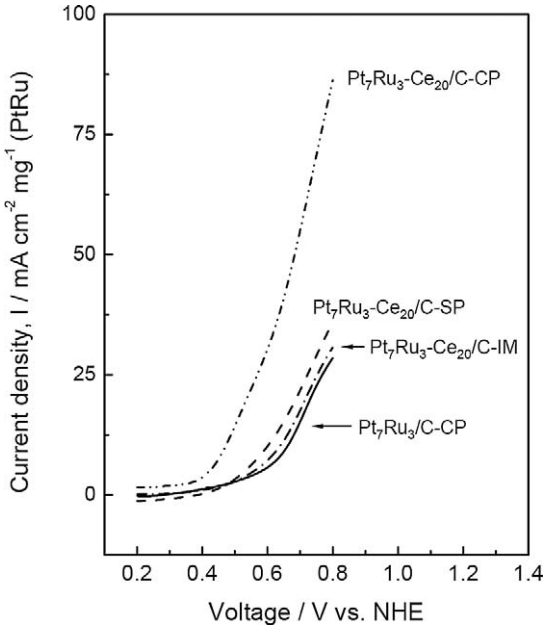

Fig. 7. Cyclic voltammograms on methanol electro-oxidation over alloy catalyst of Pt_7Ru_3/C-CP with those of CeO_2 promoted Pt_7Ru_3–Ce_{20}/C in 1.0 M CH_3OH and 0.5 M H_2SO_4.

the alloy catalysts showed an onset potential of $E_o \sim 0.35$ V (vs. NHE). Comparing the E_o (~0.60 V) of nonalloyed Pt_{10}–Ce_x/C catalysts shows that an decrease of 0.25 V in E_o was caused by Ru alloying. The decreased E_o has been attributed to a promotion of Ru to oxidize the poisoning CO into CO_2 [16]. Similar to results of Fig. 5, the addition of 20% CeO_2 to the Pt_7Ru_3/C increased its current density; however, the observed density varied with the preparation method and demonstrated the following trend at $E = 0.5$ V:

$$Pt_7Ru_3\text{–}Ce_{20}\text{/C-CP} \gg Pt_7Ru_3\text{–}Ce_{20}\text{/C-SP} > Pt_7Ru_3\text{–}Ce_{20}\text{/C-IM}. \quad (2)$$

Table 3
Catalytic activity of Pt_7Ru_3/C and Pt_7Ru_3–Ce_{20}/C toward methanol oxidation in CV characterization

Sample	E_o[a] (V)	I_{05}[b] (mA cm^{-2} mg$^{-1}_{PtRu}$)	E_{max}[c] (V)	I_{max}[d] (mA cm^{-2} mg$^{-1}_{PtRu}$)
Pt_7Ru_3/C-CP	0.39	3.7	0.97	41
Pt_7Ru_3–Ce_{20}/C-CP	0.36	14.5	1.06	137
Pt_7Ru_3–Ce_{20}/C-IM	0.30	2.9	0.97	48
Pt_7Ru_3–Ce_{20}/C-SP	0.38	3.2	0.96	43
PtRu/C(E-TEK)	0.34	11.0	1.05	114

[a] E_o: onset potential.
[b] I_{05}: current density at $E = 0.5$ V.
[c] E_{max}: peak potential.
[d] I_{max}: peak current density.

4. Discussion

4.1. Promotion effect of CeO_2

A previous report compared Ag/ZnO and Ag/CeO_2–ZnO catalysts for partial oxidation of methanol (POM) [9] and found that the activity and selectivity of Ag/ZnO for POM were significantly promoted by CeO_2. X-ray characterization of these catalysts found that dispersion of Ag particles on Ag/CeO_2–ZnO was significantly increased by CeO_2. For structure-insensitive reactions, the activity of metallic catalysts should increase with increasing dispersion of dispersed crystallites. The promotion of CeO_2 for POM was therefore attributed to an increase in Ag dispersion.

In the present study, the CP method was used to prepare all of the monometallic Pt catalysts. Fig. 5 indicates that Pt_{10}/C and ceria-added Pt_{10}–Ce_x/C exhibited a similar onset potential of $E_o = 0.60$ V for methanol oxidation. However, the current density of the oxidation by Pt_{10}/C was promoted by the addition of ceria (Table 2). The Pt particles on Pt_{10}/C had an average size of $d_{Pt} \sim 3$ nm on TEM and XRD (Table 1). Unfortunately, Pt particle cannot be distinguished in TEM photograms of Pt_{10}–Ce_x/C. In replacement, CeO_2 images were found to be aggregated on carbon support (Fig. A1 in supporting information). The absence of distinguishable Pt particles can be attributed to a decrease in their size. The average size of the Pt particles in the Pt_{10}–Ce_x/C sample might have been decreased to $d_{Pt} < 1.5$ nm because they are also XRD amorphous. Based on the experience with Ag/CeO_2–ZnO [9], Pt ions should have been reduced by Ce^{3+} during the coprecipitation step of Pt–Ce preparation through the following redox reaction:

$$Pt^{4+} + 4Ce^{3+} \rightarrow Pt + 4Ce^{4+}. \quad (3)$$

As a result, the reduced Pt crystallites should have been finely dispersed and adhered to ceria particles deposited on active carbon support.

In a voltammetric study, methanol was decomposed over prepared Pt catalysts. Current densities (I) observed from the voltammetry may be related to their activity toward the following electro-oxidation at anode [17]:

$$CH_3OH + H_2O \rightarrow CO_2 + 6H^+ + 6e^-. \quad (4)$$

Fig. 6 describes the variation of these catalysts' I_{08} (I at $E = 0.8$ V) with their Ce content (x). The variation of I_{08} can be at-

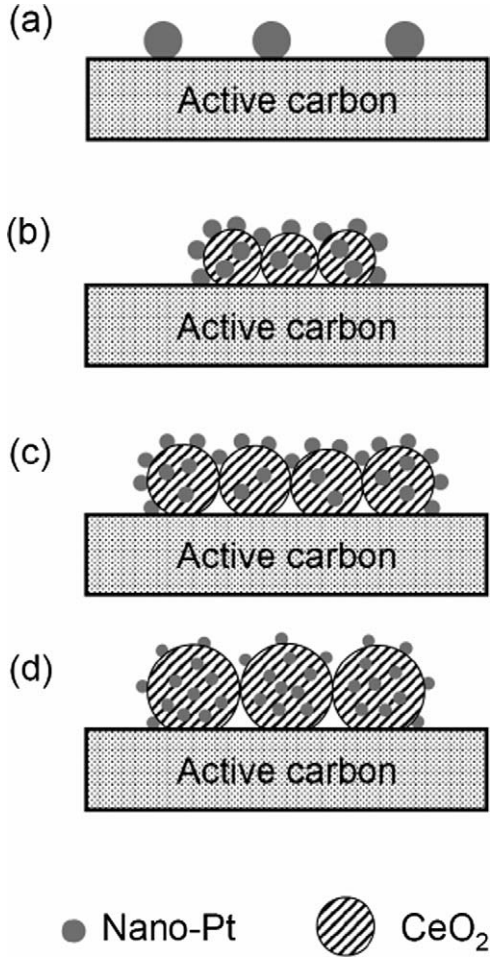

Fig. 8. Illustrative models for effects of CeO_2 loading on D_{Pt} and F_s of catalysts Pt_{10}–Ce_x/C. (a) Pt_{10}/C; (b) Pt_{10}–Ce_{10}/C; (c) Pt_{10}–Ce_{20}/C and (d) Pt_{10}–Ce_{30}/C.

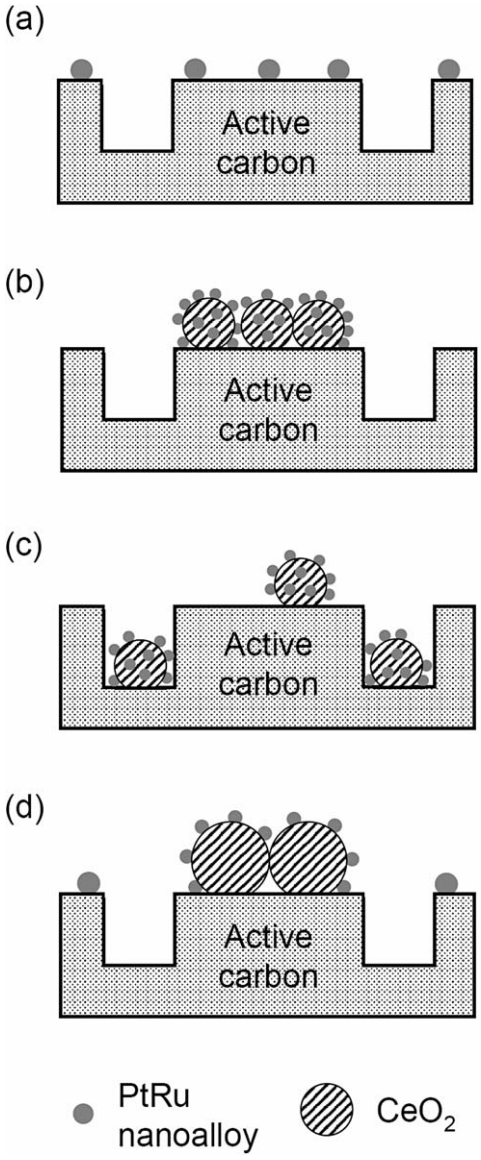

Fig. 9. The schematic models for the structure of prepared Pt_7Ru_3–Ce_x/C catalysts. (a) Pt_7Ru_3/C-CP; (b) Pt_7Ru_3–Ce_{20}/C-CP; (c) Pt_7Ru_3–Ce_{20}/C-IM; (d) Pt_7Ru_3–Ce_{20}/C-SP.

tributed to a difference in the density of Pt sites (N_{Pt}) available on Pt_{10}–Ce_x/C for reaction (4). These catalysts were prepared by the same coprecipitation method. In this coprecipitation, Pt and CeO_2 were deposited simultaneously on the carbon support. A fraction of small Pt particles ($d_{Pt} < 1.5$ nm) should have been occluded in large particles of codeposited CeO_2 ($d_{CeO_2} > 4.5$ nm). As a result, the N_{Pt} available for the catalytic reaction of methanol decomposition increased not only with the dispersion of Pt clusters (D_{Pt}) on the catalyst, but also with the fraction of the Pt clusters exposed to the CeO_2 surface (F_s). Accordingly, the variation of I_{08} with x should be proportional to D_{Pt} and F_s, that is,

$$I_{08} \propto D_{Pt} \times F_s. \quad (5)$$

Fig. 8 schematically describes speculated effects of CeO_2 loading on D_{Pt} and F_s of Pt_{10}–Ce_x/C. Pt crystallites on the nonpromoted Pt_{10}/C (Fig. 8a) had an average size of $d_{Pt} \sim 3.1$ (see row 3 in Table 1). This size suggested a dispersion of $D_{Pt} = 35\%$ on assuming that

$$D_{Pt} = 1.1/d_{Pt}\ (\text{in nm}) \quad [18]. \quad (6)$$

Evidently, two-thirds of the Pt atoms in this catalyst were not available for the decomposition reaction.

Unfortunately, the size of the Pt crystallites on CeO_2-promoted catalysts of Pt_{10}–Ce_x/C cannot be detected by the TEM and XRD characterization. A significant shrinkage of d_{Pt} by the promotion of CeO_2 (Figs. 8b, 8c, and 8d) is therefore suggested. The shrinkage of d_{Pt} is expected from reaction (3) during CP preparation. Accordingly, the initial increase of I_{08} from 30 to 50 $mA\,cm^{-2}\,mg_{Pt}^{-1}$ with x at $x \leqslant 20\%$ in Fig. 6 can be attributed to an increase in D_{Pt}. An increase in D_{Pt} may increase the rate of decomposition activity.

The amount of CeO_2 used for Pt_{10}–Ce_x/C promotion is limitated. The activity of methanol decomposition (exhibited by I_{08}) was optimized at $x = 20\%$, as shown in Fig. 6. A further increase in CeO_2 content to $x > 20\%$ decreased the I_{08} of Pt_{10}–Ce_x/C. The decrease may be tied to the loss of F_s in Eq. (5). Column 5 of Table 1 lists variations in the size of CeO_2 on Pt_{10}–Ce_x/C. The d_{CeO_2} size measured by XRD was ~5 nm for

$x = 10$ and 20%, increasing to ∼8 nm as $x = 30\%$. An increase in CeO_2 size would occlude a large fraction of platinum crystallites. Accordingly, F_s should have been substantially reduced on Pt_{10}–Ce_{30}/C (as shown in Fig. 8d).

4.2. Effect of preparation procedure on Pt_7Ru_3–Ce_x/C

Fig. 7 indicates that the current density of bimetallic Pt–Ru catalysts also increased due to coprecipitation of 20% CeO_2. Conceivably, the promotion of CeO_2 should result from increased dispersion of the Pt–Ru crystallites deposited. Three different procedures—CP (CeO_2, Pt, and Ru simultaneously and straightway deposited on carbon by NaOH), SP (Ce^{3+} predeposited on active carbon before codeposition of Pt and Ru by NaOH), and IM (Ce^{3+}, Pt^{4+}, and Ru^{3+} ions preimpregnated before their deposition by NaOH)—were used for preparation of CeO_2-promoted bimetallic catalysts. Table 1 shows that these catalysts (Pt_7Ru_3–Ce_{20}/C-CP, Pt_7Ru_3–Ce_{20}/C-IM, and Pt_7Ru_3–Ce_{20}/C-SP) had similar compositions (Pt, 5.2%; Ru, 2.4%; Ce, 16%). However, the measured profiles of I varied with the method of catalyst preparation. Column 3 of Table 3 compares I_{05} (current density at a fixed polarization of $E = 0.5$ V) for the bimetallic catalysts prepared in this study. Pt_7Ru_3–Ce_{20}/C-CP had a larger I_{05} [14.5 mA cm^{-2} mg^{-1}_{PtRu}] than those of Pt_7Ru_3–Ce_{20}/C-IM [2.9 mA cm^{-2} mg^{-1}_{PtRu}] and Pt_7Ru_3–Ce_{20}/C-SP [3.2 mA cm^{-2} mg^{-1}_{PtRu}]. Obviously, the method of catalyst preparation has a prominent effect on catalyst activity.

The variation of catalyst activity with preparation procedure can be explained by the difference in the fraction of PtRu crystallites [F_s of Eq. (5)] for methanol oxidation. Fig. 9 provides a schematic model for the structure of prepared Pt_7Ru_3–Ce_x/C catalysts. The Pt–Ru nanoalloy particles were codeposited with CeO_2 on the surface of carbon support in sample Pt_7Ru_3–Ce_{20}/C-CP (Fig. 9b). A high I_{05} (by a factor ∼4) of this catalyst compared with that of nonpromoted Pt_7Ru_3/C (Fig. 9a, also prepared by the CP method) may be attributed to the improved dispersion of alloy particles.

A large fraction of metal and CeO_2 (along with alloy particles deposited thereon) should have been impregnated into the internal pores of active carbon (pore diameter < 6 nm) in Pt_7Ru_3–Ce_{20}/C-IM. Conceivably, its low I_{05} may be attributed to the impregnation of active sites into the pores (Fig. 9c) during the preimpregnation step of preparation [19,20]. Diffusion of methanol was a serious limitation for its decomposition in CV. For the SP method, $Ce(OH)_3$ was precipitated on carbon black support before the precipitation of Pt and Ru ions. The promotion of alloy dispersion by CeO_2 was not effective in Pt_7Ru_3–Ce_{20}/C-SP (Fig. 9d).

5. Conclusion

In this work, highly dispersed 10 wt% alloy catalysts of Pt_7Ru_3/C and Pt_7Ru_3–Ce_{20}/C were prepared by the coprecipitation method. The catalytic activity of prepared catalysts toward electro-oxidation of methanol was studied by CV characterization. Based on our findings, the following conclusions can be drawn:

1. The activity of PtRu/C catalyst may be significantly promoted by codeposition of CeO_2 with Pt and Ru.
2. The promotion of CeO_2 to Pt–Ru/C catalysts may be attributed to an increase in D_M.
3. The promotion by CeO_2 is optimized at 20% in catalyst composition. A CeO_2 content of >20% may decrease the decomposition activity due to an occlusion of metal crystallites into large CeO_2 particles.
4. The procedure for preparing Pt_7Ru_3–Ce_{20}/C catalysts has a significant effect on their activity. The variation in activity may be attributed to differences in the site density of nano-PtRu available for methanol decomposition.

Acknowledgment

The authors thank the National Science Council for financial support for this study.

Supporting information

The online version of this article contains additional supplementary material.

Please visit DOI: 10.1016/j.jcat.2006.04.020.

References

[1] A.J. Appleby, F.R. Foulkes, Fuel Cell Handbook, Van Nostrand Reinhold, New York, 1989.
[2] S.-Y. Huang, S.-M. Chang, C.-T. Yeh, J. Phys. Chem. B 110 (2006) 234.
[3] R. Liu, H. Iddir, Q. Fan, G. Hou, A. Bo, K.L. Ley, E.S. Smotkin, J. Phys. Chem. B 104 (2000) 2518.
[4] Y.-C. Liu, X.-P. Qiu, Y.-Q. Huang, W.-T. Zhu, J. Power Sources 111 (2002) 160.
[5] P. Stonehart, P.N. Ross, Catal. Rev. Sci. Eng. 12 (1975) 1.
[6] Z. Jusys, T.J. Schmidt, L. Dubau, K. Lasch, J. Garche, R.J. Behm, J. Power Sources 105 (2002) 297.
[7] W.T. Napporn, H. Laborde, J.-M. Léger, C. Lamy, J. Electroanal. Chem. 404 (1996) 153.
[8] T. Frelink, W. Visscher, A.P. Cox, J.A.R. Van Veen, Electrochim. Acta 40 (1995) 1537.
[9] L. Mo, X. Zheng, C.T. Yeh, Chem. Commun. (2004) 1426.
[10] M. Kang, M.W. Song, C.H. Lee, Appl. Catal. A 251 (2003) 143.
[11] X. Tang, B. Zhang, Y. Li, Y. Xu, Q. Xin, W. Shen, Catal. Today 93 (2004) 191.
[12] C. Xu, P.K. Shen, J. Power Sources 142 (2005) 27.
[13] H.B. Yu, J.H. Kim, H.I. Lee, M.A. Scibioh, J. Lee, J. Han, S.P. Yoon, H.Y. Ha, J. Power Sources 140 (2005) 59.
[14] C. Xu, P.K. Shen, Chem. Commun. (2004) 2238.
[15] From JCPDS data.
[16] K.-W. Park, J.-H. Choi, S.-A. Lee, C. Pak, H. Chang, Y.-E. Sung, J. Catal. 224 (2004) 236.
[17] M.P. Hogarth, T.R. Ralph, Platinum Met. Rev. 46 (2002) 146.
[18] J.M. Garcia-Cortes, J. Perez-Ramirez, M.J. Illan-Gomez, C. Salinas-Martinez de Lecea, Catal. Commun. 4 (2003) 165.
[19] D.R. Rolison, Science 299 (2003) 1698.
[20] V. Raghuveer, A. Manthiram, Electrochem. Solid-State Lett. 7 (2004) A336.